JNeurosci
THE JOURNAL OF NEUROSCIENCE

Research Articles: Behavioral/Cognitive

Asymmetric frequency-specific feedforward and feedback information flow between hippocampus and prefrontal cortex during verbal memory encoding and recall

https://doi.org/10.1523/JNEUROSCI.0802-21.2021

Cite as: J. Neurosci 2021; 10.1523/JNEUROSCI.0802-21.2021

Received: 14 April 2021
Revised: 5 July 2021
Accepted: 21 July 2021

Asymmetric frequency-specific feedforward and feedback information flow between hippocampus and prefrontal cortex during verbal memory encoding and recall

Anup Das[1] *and Vinod Menon*[1,2,3]

Department of Psychiatry & Behavioral Sciences[1]

Department of Neurology & Neurological Sciences[2]

Stanford Neurosciences Institute[3]

Stanford University School of Medicine

Stanford, CA 94305

Title (50-word maximum): Asymmetric frequency-specific feedforward and feedback information flow between hippocampus and prefrontal cortex during verbal memory encoding and recall

Abbreviated title (50-character maximum): Hippocampal-prefrontal cortex information flow

Author names and affiliations, including postal codes:

Anup Das, Department of Psychiatry & Behavioral Sciences, Stanford University School of Medicine, Stanford, CA 94305

Vinod Menon, Department of Psychiatry & Behavioral Sciences, Department of Neurology & Neurological Sciences, and Stanford Neurosciences Institute, Stanford University School of Medicine, Stanford, CA 94305

Corresponding author email address: a1das@stanford.edu, menon@stanford.edu

Number of pages: 51

Number of figures: 11

Number of tables: 3

Number of words in Abstract: 238

Number of words in Introduction: 1361

Number of words in Discussion: 1965

Conflict of interest statement: The authors declare no competing financial interests.

Acknowledgements

We are grateful to members of the UPENN-RAM consortia for generously sharing their unique iEEG data. We thank Drs. Paul A. Wanda, Michael V. DePalatis, Youssef Ezzyat, Richard Betzel, and Leon A. Davis for assistance with the UPENN-RAM dataset. We thank Drs. Matteo Fraschini and Arjan Hillebrand for generously sharing their MATLAB code for phase transfer entropy analysis, and Dr. Byeongwook Lee for assistance with Figure 1. This research was supported by NIH grants NS086085 and EB022907.

Abstract

Hippocampus and prefrontal cortex (PFC) circuits are thought to play a prominent role in human episodic memory, but the precise nature, and electrophysiological basis, of directed information flow between these regions and their role in verbal memory formation has remained elusive. Here we investigate nonlinear causal interactions between hippocampus and lateral PFC using intracranial EEG recordings (from both sexes) during verbal memory encoding and recall tasks. Direction-specific information theoretic analysis revealed higher causal information flow from the hippocampus to PFC than in the reverse direction. Crucially, this pattern was observed during both memory encoding and recall, and the strength of causal interactions was significantly greater during memory task performance than resting baseline. Further analyses revealed frequency-specificity of interactions with greater causal information flow from hippocampus to the PFC in the delta-theta frequency band (0.5-8 Hz); in contrast, PFC to hippocampus causal information flow were stronger in the beta band (12-30 Hz). Across all hippocampus-PFC electrode pairs, propagation delay between the source and target signals was estimated to be 17.7 msec, which is physiologically meaningful and corresponds to directional signal interactions on a timescale consistent with monosynaptic influence. Our findings identify distinct asymmetric feedforward and feedback signaling mechanisms between the hippocampus and PFC and their dissociable roles in memory recall, demonstrate that these regions preferentially use different frequency channels, and provide novel insights into the electrophysiological basis of directed information flow during episodic memory formation in the human brain.

Significance Statement

Hippocampal-prefrontal cortex circuits play a critical role in episodic memory in rodents, non-human primates, and humans. Investigations using noninvasive functional magnetic resonance imaging techniques have provided insights into coactivation of the hippocampus and PFC during memory formation, however, the electrophysiological basis of dynamic causal hippocampal-PFC interactions in the human brain are poorly understood. Here, we use data from a large cohort of intracranial EEG recordings to investigate the neurophysiological underpinnings of asymmetric feedforward and feedback hippocampal-prefrontal cortex interactions and their nonlinear causal dynamics during both episodic memory encoding and recall. Our findings provide novel insights into the electrophysiological basis of directed bottom-up and top-down information flow during episodic memory formation in the human brain.

Introduction

Hippocampal-prefrontal cortex (PFC) circuits play a critical role in episodic memory in rodents, non-human primates, and humans (Eichenbaum, 2017; Rutishauser, Reddy, Mormann, & Sarnthein, 2021). Impairments in hippocampal-PFC circuit interactions are prominent in psychiatric and neurological disorders (Dickerson & Eichenbaum, 2010; Meyer-Lindenberg et al., 2005; Uhlhaas & Singer, 2012), highlighting a critical need for understanding of their electrophysiological mechanisms in the human brain. In the past decade, investigations using noninvasive functional magnetic resonance imaging (fMRI) techniques have provided consistent evidence for coactivation of the hippocampus and multiple PFC subdivisions during a wide range of tasks involving memory encoding and recall (Moscovitch, Cabeza, Winocur, & Nadel, 2016; Rugg & Vilberg, 2013). However, the electrophysiological basis of dynamic causal hippocampal-PFC interactions in the human brain are poorly understood as fMRI does not have the requisite temporal resolution to address this question. Here, we use data from a large cohort of intracranial EEG (iEEG) recordings to investigate feedforward and feedback causal information flow between the hippocampus and distinct subdivisions of the PFC, and its frequency specificity, during memory encoding and subsequent recall of verbal materials. We operationalize causality as follows: a brain region has a causal influence on a target if knowing the past history of temporal signals in both regions improves the ability to predict the target's signal in comparison to knowing only the target's past (Granger, 1969; Lobier, Siebenhühner, Palva, & Matias, 2014) (see **Methods**).

Multiple lines of evidence from studies in rodents and non-human primates have pointed to tight anatomical and functional links between hippocampus and PFC as key neural pathways for memory and learning. Anterograde and retrograde tracing studies in rodents have uncovered projections from the hippocampus to the PFC (Hoover & Vertes, 2007; Jay & Witter, 1991). Similarly, studies in rhesus monkeys have demonstrated direct tracts linking the hippocampus to the PFC (Goldman-Rakic, Selemon, & Schwartz, 1984; Lavenex & Amaral, 2000). Recent studies using diffusion-weighted imaging and resting-state fMRI have confirmed intrinsic hippocampus connectivity with the PFC in both macaques and humans (Croxson et al., 2005; Qin et al., 2016).

In conjunction with delineation of anatomical tracts between the hippocampus and PFC, electrophysiological studies in rodents have reported strong theta (4-8 Hz) and delta (0.5-4 Hz) frequency band oscillations in the hippocampus (Eichenbaum, 2017; Roy, Svensson, Mazeh, & Kocsis, 2017; Schultheiss et al., 2020; Siapas, Lubenov, & Wilson, 2005). Rodent electrophysiological studies have also revealed synchronized activity between hippocampus and PFC in these frequency bands during spatial memory tasks (Benchenane et al., 2010; Jones & Wilson, 2005; Place, Farovik, Brockmann, & Eichenbaum, 2016; Simons & Spiers, 2003; Spiers, 2020). Compared to studies in rodents, the electrophysiological signatures of hippocampal-PFC circuits have been less well investigated in non-human primates, but recent reports have emphasized bidirectional information flow between the hippocampus and PFC associated with accurate spatial memory performance (Brincat & Miller, 2015; Cruzado, Tiganj, Brincat, Miller, & Howard, 2020). Together, these findings suggest that coordinated interactions between the

hippocampus and PFC are critical for spatial learning and memory across species (Eichenbaum, 2017).

In humans, a large body of fMRI studies have consistently reported coactivation of the hippocampus and multiple PFC regions during both spatial and verbal memory tasks (Dickerson & Eichenbaum, 2010; Dobbins, Foley, Schacter, & Wagner, 2002; Moscovitch et al., 2016; Qin et al., 2014; Rugg & Vilberg, 2013; Simons & Spiers, 2003), and hippocampus-PFC coactivation is also associated with better memory performance (Kumaran, Summerfield, Hassabis, & Maguire, 2009). Various measures of functional connectivity between the hippocampus and PFC have also been associated with memory recall (Preston & Eichenbaum, 2013; Qin et al., 2014; van Kesteren, Fernandez, Norris, & Hermans, 2010), but their electrophysiological basis are poorly understood. Studies using non-invasive magnetoencephalography in humans have suggested that hippocampal-PFC coherence in the delta-theta frequency band is associated with successful memory integration (Backus, Schoffelen, Szebenyi, Hanslmayr, & Doeller, 2016; Guitart-Masip et al., 2013; Spaak & de Lange, 2020). Studies using iEEG have reported increased hippocampal-PFC theta band synchronization associated with spatial memory retrieval (Ekstrom & Watrous, 2014; Neuner et al., 2014; Watrous, Tandon, Conner, Pieters, & Ekstrom, 2013) and have hinted that a similar process may apply to verbal memory recall as well (Anderson, Rajagovindan, Ghacibeh, Meador, & Ding, 2010).

Although these studies have provided significant insights into hippocampal and PFC engagement in human episodic memory, the precise pattern of "bottom-up" and "top-down" dynamic causal interactions and frequency dependent direction of information flow are not known due to the

poor temporal resolution of fMRI and paucity of deep brain electrophysiological data from multiple brain regions. Furthermore, compared to spatial memory, there have been comparatively far fewer investigations of hippocampal-PFC interactions associated with episodic memory encoding and recall of verbal materials, a domain with no equivalents in rodent and non-human primate models. To address this challenge, we used iEEG data from the UPENN-RAM study (Solomon et al., 2019), which includes depth recordings sampled at a high temporal resolution of 1KHz from a large cohort of individuals, to probe the directionality of information flow between the hippocampus and multiple subdivisions of the left lateral PFC.

The first goal of our study was to determine directed causal information flow between the hippocampus and PFC during verbal episodic memory. We investigated the directionality of information flow between these regions during encoding and subsequent recall of a list of words using phase transfer entropy (PTE) (Hillebrand et al., 2016; Lobier et al., 2014; Wang et al., 2017). PTE provides a robust and powerful measure for characterizing information flow between brain regions based on phase coupling and, crucially, it captures linear as well as nonlinear intermittent and nonstationary causal dynamics in iEEG data (Hillebrand et al., 2016; Lobier et al., 2014; Menon et al., 1996).

Our analysis focused on hippocampus interactions with two distinct PFC areas encompassing inferior frontal gyrus (IFG) and middle frontal gyrus (MFG) in left hemisphere regions which have been implicated in prior fMRI studies of verbal episodic memory (Dobbins et al., 2002; Wagner, Pare-Blagoev, Clark, & Poldrack, 2001). We hypothesized that the hippocampus would show directional causal influence on the PFC, when compared to resting baseline. We further

predicted that causal influences of the hippocampus on the PFC would be stronger, compared to the reverse direction, during memory encoding; in contrast, causal influences of IFG subdivision of the PFC on the hippocampus would be stronger, compared to the reverse direction, during memory recall based on the hypothesized role of this region in controlled memory retrieval (Badre, Poldrack, Paré-Blagoev, Insler, & Wagner, 2005; Badre & Wagner, 2007; Dobbins et al., 2002; Hasegawa, Hayashi, & Miyashita, 1999; Wagner et al., 2001).

Our second goal was to investigate the frequency-specificity of causal interactions between the hippocampus and PFC. Although no consensus has emerged on the role of specific frequencies in synchronization of neural responses between the hippocampus and PFC (Brincat & Miller, 2015; Lam, Schoffelen, Udden, Hulten, & Hagoort, 2016; Moreno, Morris, & Canals, 2016; Schoffelen et al., 2017), studies in rodents, non-human primates, and humans have pointed to prominent functional roles of the delta-theta rhythm (0.5-8 Hz) in the hippocampus (Ekstrom & Watrous, 2014; Neuner et al., 2014; Watrous et al., 2013) and beta-band rhythm (12-30 Hz) in prefrontal and parietal cortices (Boran et al., 2019; Brovelli et al., 2004; Engel & Fries, 2010; Spitzer & Haegens, 2017; Stanley, Roy, Aoi, Kopell, & Miller, 2018). This has led to the suggestion that delta-theta oscillations may preferentially contribute to synchronization of the hippocampus with the PFC (Ekstrom & Watrous, 2014), while beta band oscillations synchronize the PFC with other cortical and subcortical brain areas (Engel & Fries, 2010; Spitzer & Haegens, 2017). However, the frequency-specificity of causal interactions between the hippocampus and PFC in these two frequency bands associated with verbal memory formation has not been directly examined before. Based on the emerging literature, we test the hypothesis that the hippocampus has a stronger feedforward causal influence on the PFC in the delta-theta

band while the PFC has stronger "top-down" causal influence on the hippocampus in the beta band.

Our analysis revealed novel, behaviorally and functionally relevant, insights into the neurophysiological basis of the human hippocampal-PFC interactions and its role in both memory encoding and recall.

Methods

UPENN-RAM iEEG recordings

iEEG recordings from 102 patients shared by Kahana and colleagues at the University of Pennsylvania (UPENN) (obtained from the UPENN-RAM public data release under release ID "Release_20171012", released on 12 October, 2017) were used for analysis (Jacobs et al., 2016). Patients with pharmaco-resistant epilepsy underwent surgery for removal of their seizure onset zones. iEEG recordings of these patients were downloaded from a UPENN-RAM consortium hosted data sharing archive (URL: http://memory.psych.upenn.edu/RAM). Prior to data collection, research protocols and ethical guidelines were approved by the Institutional Review Board at the participating hospitals and informed consent was obtained from the participants and guardians (Jacobs et al., 2016). Details of all the recordings sessions and data pre-processing procedures are described by Kahana and colleagues (Jacobs et al., 2016). Briefly, iEEG recordings were obtained using subdural grids and strips (contacts placed 10 mm apart) or depth electrodes (contacts spaced 5–10 mm apart) using recording systems at each clinical site. iEEG

systems included DeltaMed XlTek (Natus), Grass Telefactor, and Nihon-Kohden EEG systems. Electrodes located in brain lesions or those which corresponded to seizure onset zones or had significant interictal spiking or had broken leads, were excluded from analysis.

Anatomical localization of electrode placement was accomplished by co-registering the postoperative computed CTs with the postoperative MRIs using FSL (FMRIB (Functional MRI of the Brain) Software Library), BET (Brain Extraction Tool), and FLIRT (FMRIB Linear Image Registration Tool) software packages. Preoperative MRIs were used when postoperative MRIs were not available. The resulting contact locations were mapped to MNI space using an indirect stereotactic technique and OsiriX Imaging Software DICOM viewer package. We used the Brainnetome atlas (Fan et al., 2016) to demarcate the IFG, MFG, and the hippocampus (Greicius et al., 2003). Other important brain regions such as the dorsal anterior cingulate cortex (dACC) and the dorsal medial prefrontal cortex (dmPFC) were excluded from analysis due to lack of sufficient electrode placement in these areas. Out of 102 individuals, data from 26 individuals (aged from 18 to 61, mean age 37.7 ± 13.7, 16 females) were used for subsequent analysis based on electrode placement in IFG, MFG, and the hippocampus. Gender differences were not analyzed in this study due to lack of sufficient male participants for electrodes pairs for brain regions (for example, hippocampus-IFG and hippocampus-MFG had only 2 male patients each, **Table 2**).

iEEG signals were sampled at 1,000 Hz. The two major concerns when analyzing interactions between closely spaced intracranial electrodes are volume conduction and confounding interactions with the reference electrode (Burke et al., 2013). Hence bipolar referencing was used

267 to eliminate confounding artifacts and improve the signal-to-noise ratio of the neural signals,
268 consistent with previous studies using UPENN-RAM iEEG data (Burke et al., 2013; Ezzyat et
269 al., 2018). Signals recorded at individual electrodes were converted to a bipolar montage by
270 computing the difference in signal between adjacent electrode pairs on each strip, grid, and depth
271 electrode and the resulting bipolar signals were treated as new "virtual" electrodes originating
272 from the midpoint between each contact pair, identical to procedures in previous studies using
273 UPENN-RAM data (Solomon et al., 2019). Line noise (60 Hz) and its harmonics were removed
274 from the bipolar signals and finally each bipolar signal was Z-normalized by removing mean and
275 scaling by the standard deviation. For filtering, we used a fourth order two-way zero phase lag
276 Butterworth filter throughout the analysis.
277
278 ***iEEG verbal memory encoding and recall, and resting-state task conditions***
279
280 Patients performed multiple trials of a "free recall" experiment, where they were presented with
281 a list of words and subsequently asked to recall as many as possible from the original list (**Figure**
282 **1**). Details of the task are described elsewhere (Solomon et al., 2017; Solomon et al., 2019).
283 Average recall accuracy across patients was 25.5% ± 8.7%, similar to prior studies of verbal
284 episodic memory retrieval in neurosurgical patients (Burke et al., 2014). The mismatch in the
285 number trials therefore made it difficult to directly compare causal signaling measures between
286 successfully versus unsuccessfully recalled words. From the point of view of probing
287 behaviorally effective memory encoding our focus was therefore on successful recall consistent
288 with most prior studies (Long, Burke, & Kahana, 2014; Watrous et al., 2013). We analyzed
289 iEEG epochs from the encoding and recall periods of the "free recall" task as well as inter-trial

intervals when participants were given no explicit cognitive task, similar to previous iEEG studies (Horak et al., 2017; Miller, Weaver, & Ojemann, 2009; Norman, Yeagle, Harel, Mehta, & Malach, 2017; Yanagisawa et al., 2012). For resting-state, we extracted 10-second iEEG recordings (epochs) prior to the beginning of each trial. To reduce boundary and carry over effects, we discarded 3 seconds each of iEEG data from the beginning and end of each epoch, resulting in multiple 4 second epochs (Das & Menon, 2020). The encoding and recall epochs were 30-seconds for each trial. Each encoding trial consisted of 12 words each of 1.6-second duration (**Figure 1**). For the recall periods, iEEG recordings 1.6-second prior to the vocal onset of each word were analyzed (Solomon et al., 2019). Data from each trial was analyzed separately and specific measures were averaged across trials. The duration of memory encoding and recall, and resting-state trials were matched to preclude trial-length effects.

iEEG analysis of power spectral density

To calculate average power, we first filtered the iEEG time-series in the frequency band of interest and power, after removing the linear trend, was calculated as the sum of the squares of the amplitudes of the iEEG time-series divided by the length of the time-series.

iEEG analysis of phase transfer entropy (PTE) and causal dynamics

Phase transfer entropy (PTE) is a nonlinear measure of the directionality of information flow between time-series and can be applied as a measure of causality to nonstationary time-series (Lobier et al., 2014). Note that information flow described here relates to signaling between

brain areas and does not necessarily reflect the representation or coding of behaviorally relevant variables per se. The PTE measure is in contrast to the Granger causality measure which can be applied only to stationary time-series (Barnett & Seth, 2014). We first carried out a stationarity test of the iEEG recordings (unit root test for stationarity (Barnett & Seth, 2014)) and found that the spectral radius of the autoregressive model is very close to one, indicating that the iEEG time-series is nonstationary. This precluded the applicability of the Granger causality analysis in our study.

Given two time-series $\{x_i\}$ and $\{y_i\}$, where $i = 1, 2, ..., M$, instantaneous phases were first extracted using the Hilbert transform. Let $\{x_i^p\}$ and $\{y_i^p\}$, where $i = 1, 2, ..., M$, denote the corresponding phase time-series. If the uncertainty of the target signal $\{y_i^p\}$ at delay τ is quantified using Shannon entropy, then the PTE from driver signal $\{x_i^p\}$ to target signal $\{y_i^p\}$ can be given by

$$PTE_{x\to y} = \sum_i p\left(y_{i+\tau}^p, y_i^p, x_i^p\right) \log\left(\frac{p\left(y_{i+\tau}^p \mid y_i^p, x_i^p\right)}{p\left(y_{i+\tau}^p \mid y_i^p\right)}\right), \quad \text{(i)}$$

where the probabilities can be calculated by building histograms of occurrences of singles, pairs, or triplets of instantaneous phase estimates from the phase time-series (Hillebrand et al., 2016). For our analysis, the number of bins in the histograms was set as $3.49 \times STD \times M^{-1/3}$ and delay τ was set as $2M / M_{\pm}$, where STD is average standard deviation of the phase time-series $\{x_i^p\}$ and $\{y_i^p\}$ and $M_{\pm}$ is the number of times the phase changes sign across time and channels

(Hillebrand et al., 2016). PTE has been shown to be robust against the choice of the delay τ and the number of bins for forming the histograms (Hillebrand et al., 2016).

Statistical analysis

Statistical analysis was conducted using mixed effects analysis with the lmerTest package (Kuznetsova, Brockhoff, & Christensen, 2017) implemented in R software (version 4.0.2, R Foundation for Statistical Computing). Because PTE data were not normally distributed, we used BestNormalize (Peterson & Cavanaugh, 2018) which contains a suite of transformation-estimating functions that can be used to optimally normalize data. The resulting normally distributed data were subjected to mixed effects analysis with the following model: *PTE ~ Condition + (1|Subject)*, where *Condition* models the fixed effects (condition differences) and (1|*Subject*) models the random repeated measurements within the same participant. Analysis of variance (ANOVA) was used to test the significance of findings with FDR-corrections for multiple comparisons ($p<0.05$). Similar mixed effects statistical analysis procedures were used for comparison of power spectral density across task conditions.

Finally, we conducted surrogate analysis to test the significance of the estimated PTE values (Hillebrand et al., 2016). The estimated phases from the Hilbert transform for electrodes from a given pair of brain areas were time-shuffled so that the predictability of one time-series from another is destroyed, and PTE analysis was repeated on this shuffled data to build a distribution of surrogate PTE values against which the observed PTE was tested ($p<0.05$).

Results

Causal information flow from the hippocampus to PFC during successful memory encoding

We first examined dynamic causal influences of the hippocampus on the inferior frontal gyrus (IFG) and middle frontal gyrus (MFG) nodes of the PFC during the memory encoding period of a verbal episodic memory task in which participants were presented with a sequence of words and asked to remember them for subsequent recall (**Methods**, **Tables 1-2**, **Figures 1a, b**). Briefly, the task consisted of three periods: encoding, delay, and recall. During encoding, a list of 12 words was visually presented for ~30 s. Words were selected at random, without replacement, from a pool of high frequency English nouns (http://memory.psych.upenn.edu/Word_Pools). Each word was presented for a duration of 1600 msec, followed by an inter-stimulus interval of 800 to 1200 msec. After a 20 sec post-encoding delay, participants were instructed to recall as many words as possible during the 30 sec recall period.

We used phase transfer entropy (PTE) (Lobier et al., 2014) to compute broadband (0.5-160 Hz) causal influence from the hippocampus to the IFG and MFG in the PFC and vice-versa. During successful memory encoding, the hippocampus had higher broadband causal influences on both the IFG ($F(1, 187) = 41.79$, $p<0.001$) and MFG ($F(1, 346) = 80.33$, $p<0.001$) nodes than the reverse (**Figures 2a, b** respectively). However, causal influence of the hippocampus on the IFG and MFG nodes did not differ from each other during successful memory encoding ($F(1, 271) = 0.11$, $p>0.05$). Causal influence of the IFG on the hippocampus was higher than the causal influence of the MFG on the hippocampus during successful memory encoding ($F(1, 274) =$

24.14, $p<0.001$). These results demonstrate that the hippocampus has asymmetric causal information flow to both the IFG and MFG during successful memory encoding.

Causal information flow from the hippocampus on PFC during successful memory recall

Next, we examined causal influences of the hippocampus on the PFC during the recall phase of the verbal episodic memory task in which participants recalled the words they had seen during the memory encoding phase (**Figure 1b**, **Methods**). During successful memory recall, the hippocampus had higher broadband causal influences on both the IFG ($F(1, 187) = 40.47$, $p<0.001$) and MFG ($F(1, 346) = 70.69$, $p<0.001$) than the reverse (**Figures 2a, b** respectively). However, causal influence of the hippocampus on the IFG and MFG did not differ from each other during successful memory recall ($F(1, 271) = 0.01$, $p>0.05$). Causal influence of the IFG on the hippocampus was higher than the causal influence of the MFG on the hippocampus during successful memory recall ($F(1, 274) = 28.91$, $p<0.001$). These results demonstrate that the hippocampus has asymmetric causal information flow to both the IFG and MFG subdivisions of the PFC during successful memory recall.

Causal information flow from the hippocampus on PFC during memory encoding and memory recall, compared to resting state

We next investigated changes in causal influences of the hippocampus on the IFG and MFG during memory encoding and recall, compared to the resting-state. Our analysis revealed that the causal influences of the hippocampus on the IFG and MFG were higher during both the

successful memory encoding and recall task conditions, in comparison to the resting-state ($F(1, 187) = 28.70$, $F(1, 187) = 11.94$, $F(1, 346) = 57.65$, $F(1, 346) = 32.05$ respectively; $p<0.001$ in all cases) (**Figure 3**). These results demonstrate that the hippocampus has asymmetric causal information flow to both the IFG and MFG during task conditions compared to resting baseline.

Causal information flow from the hippocampus to PFC in the delta-theta frequency band

Based on previous findings from iEEG studies which have reported significant delta-theta frequency (0.5-8 Hz) band activity in the hippocampus during recall of verbal, temporal and spatial information from recently encoded memories and hippocampal-PFC interactions during spatial memory recall (Ekstrom & Watrous, 2014; Neuner et al., 2014; Watrous et al., 2013), we next investigated the dynamic causal influences of the hippocampus on the PFC nodes and vice-versa in the low frequency delta-theta (0.5-8 Hz) band (see **Figure 5** for results in the 0.5-12 Hz frequency band). We computed PTE from the PFC nodes to the hippocampus and, in the reverse direction, during successful memory encoding, and recall in the delta-theta (0.5-8 Hz) frequency band. This analysis revealed that the hippocampus had higher causal influences on the IFG and MFG subdivisions of the PFC than the reverse during both successful memory encoding and recall conditions ($F(1, 185) = 30.83$, $F(1, 186) = 11.68$, $F(1, 345) = 66.30$, $F(1, 345) = 48.34$ respectively; $p<0.001$ in all cases) (**Figure 4**). These results demonstrate a key role for delta-theta frequency signaling underlying higher causal influences of the hippocampus on the PFC.

Causal information from the PFC to the hippocampus in the beta frequency band

Next, we examined frequency specific information flow between the hippocampus and PFC based on emerging findings in non-human primates regarding cortical signaling in the beta frequency (12-30 Hz) band during cognition (Engel & Fries, 2010). We computed PTE from the PFC nodes to the hippocampus, and in the reverse direction, during successful memory encoding, and recall in the beta frequency (12-30 Hz) band. This analysis revealed that the IFG had higher causal influences on the hippocampus during both successful memory encoding ($F(1, 189) = 62.13$, $p<0.001$) and recall conditions ($F(1, 189) = 24.72$, $p<0.001$). Similarly, the MFG also had higher causal influences on the hippocampus during both successful memory encoding ($F(1, 346) = 59.14$, $p<0.001$) and recall ($F(1, 345) = 6.03$, $p<0.05$)) (**Figure 6**). These results demonstrate a key role for beta frequency signaling underlying higher causal influences of both the IFG and MFG subdivisions of the PFC on the hippocampus.

Surrogate data analysis of causal information flow between the hippocampus and the PFC

Finally, we conducted surrogate data analysis to test the significance of the estimated PTE values compared to PTE expected by chance (**Methods**). The estimated phases from the Hilbert transform for electrodes from pairs of brain areas were time-shuffled and PTE analysis was repeated on this shuffled data to build a distribution of surrogate PTE values against which the observed PTE was tested. This analysis revealed that causal information flow from the hippocampus to the IFG and MFG nodes and the reverse were significantly higher than those expected by chance (**Figure 7**) ($p<0.05$ in all cases) in broadband for both successful memory

encoding and recall, indicating bidirectional causal information flow between the hippocampus and the PFC in broadband.

Frequency-specific surrogate data analysis further revealed that causal information flow from the hippocampus to the IFG and MFG nodes and the reverse were significantly higher than those expected by chance (**Figure 8**) ($p<0.05$ in all cases) in the delta-theta frequency band for both successful memory encoding and recall, indicating bidirectional causal information flow between the hippocampus and the PFC in delta-theta band. Analysis in the beta frequency band revealed that causal information flow from the hippocampus to the IFG and MFG nodes and the reverse were significantly lower than those expected by chance (**Figure 9**) ($p<0.05$ in all cases) for both successful memory encoding and recall, indicating significantly lower predictability of one brain area from the other than expected by chance, in this frequency band.

These results demonstrate that all reported effects in this study arise from causal signaling that is significantly enhanced above chance levels.

Power spectral density during memory encoding and recall compared to resting-state

Finally, we compared the power spectral density (**Methods**, **Table 3**) in the hippocampus and the IFG and MFG nodes of the PFC across resting-state, memory encoding, and memory recall conditions. As with analyses reported above, the duration of task and rest trials were matched to ensure that differences in network dynamics could not be explained by the differences in the

duration of the trials. This analysis revealed that power across the three conditions do not differ from each other in any region (hippocampus/IFG/MFG) (all *ps*>0.05).

Previous studies have suggested that power in the high-gamma band (80-160 Hz) is correlated with fMRI BOLD signals (Hutchison, Hashemi, Gati, Menon, & Everling, 2015; Lakatos, Gross, & Thut, 2019; Leopold, Murayama, & Logothetis, 2003; Mantini, Perrucci, Del Gratta, Romani, & Corbetta, 2007; Scholvinck, Maier, Ye, Duyn, & Leopold, 2010), and is thought to reflect local activity (Canolty & Knight, 2010). The spectrogram for each brain region, estimated using the short-time Fourier transform (Zhou et al., 2019), confirmed significant high-gamma band activity during both memory encoding and recall (**Figures 10** and **11** respectively). We compared high-gamma band power spectral density (see **Methods** for details) in the hippocampus and the IFG and MFG across resting-state, memory encoding, and memory recall conditions. This analysis revealed that power across the three conditions did not differ from each other in any of the three regions (all *ps*>0.05).

Discussion

We examined the electrophysiological basis of directed information flow between the hippocampus and PFC during memory formation in humans using depth iEEG recordings from the UPENN-RAM cohort (Solomon et al., 2019). Leveraging one of the largest samples to date, from 26 participants, 187 electrodes, and 276 electrode pairs, our analysis first focused on broadband signatures of causal interaction, as investigations using canonically defined frequency bands can miss aperiodic (1/f) components that might have major influence on signaling between

493 brain regions (Donoghue et al., 2020). Direction-specific information theoretic analysis revealed
494 that the hippocampus has higher causal influence on both the left hemisphere IFG and MFG
495 subdivisions of the PFC than the reverse, and this pattern was observed during both the encoding
496 and recall phases of the verbal episodic memory task. Causal information flow from the
497 hippocampus to PFC increased significantly during memory processing, compared to resting
498 baseline and surrogate data analysis revealed that the strength of information flow was
499 significantly above chance levels.
500
501 Our analysis further revealed frequency specificity of hippocampus-PFC interactions and a
502 dissociation between feedforward and top-down information flow in the delta-theta and beta
503 bands. We found that feedforward causal influences from the hippocampus to PFC in the delta-
504 theta frequency band were higher, compared to the reverse direction, during both memory
505 encoding and memory recall. In contrast, top-down causal influences from the PFC to
506 hippocampus were higher, compared to the reverse direction, in the beta frequency band during
507 both memory encoding and memory recall. Our findings provide novel insights into asymmetric
508 directionality of information flow between the hippocampus and the PFC during episodic
509 memory formation in the human brain.
510
511 *Directionality of information flow between the hippocampus and the PFC during verbal memory*
512 *formation*
513
514 The first goal of our study was to characterize the directionality of information flow between the
515 hippocampus and the PFC during cognition. Our analysis focused on left hemisphere

hippocampus, IFG, and MFG aligned with hemisphere lateralization of verbal episodic and semantic memory processes (Dobbins et al., 2002; Wagner et al., 2001). The left hippocampus and PFC are coactivated during encoding and recall of verbal stimuli in memory (Preston & Eichenbaum, 2013; Qin et al., 2014; van Kesteren et al., 2010). However, the directionality of information flow between the hippocampus and PFC during memory encoding and recall is not well understood as fMRI, the mainstay of hippocampus-PFC investigations in humans, lacks requisite temporal resolution for probing causal circuit dynamics.

To address this question, we used phase transfer entropy (PTE), which provides a robust and powerful tool for characterizing information flow between brain regions based on phase coupling (Hillebrand et al., 2016; Lobier et al., 2014; Wang et al., 2017). We used PTE rather than phase locking or coherence which have been used previously to probe hippocampal-PFC interactions in rodents (Benchenane et al., 2010; Jones & Wilson, 2005), since phase locking or coherence measures do not probe causal influences and cannot address how one region drives another. Instead, our study examined the direction of information flow between the hippocampus and the PFC using robust estimators of the direction of information flow. PTE assesses with the ability of one time-series to predict future values of other time-series thus estimating the time-delayed causal influences between the two time-series whereas phase locking or coherence can only estimate “instantaneous” phase synchronization, but not predict the future time-series. Crucially, PTE is a robust, nonlinear measure of directionality of information flow between time-series (Hillebrand et al., 2016; Lobier et al., 2014). A brain region has a stronger causal influence on a target if knowing the past phase of signals in both regions improves the ability to predict the target’s phase in comparison to knowing only the target’s past phase. PTE has several

advantages over Granger causal analysis (Barnett & Seth, 2014), as it (i) can capture nonlinear interactions, (ii) can estimate causality between nonstationary time-series, (iii) is more accurate and computationally less expensive than transfer entropy, and (iv) estimates causal interactions based on phase, rather than amplitude, coupling (Hillebrand et al., 2016; Lobier et al., 2014; Schreiber, 2000).

We examined causal influences between the hippocampus and the PFC during a verbal episodic memory task in which participants had to subsequently recall a list of words (Solomon et al., 2019). Average recall accuracy across patients was 25.5% ± 8.7%, similar to prior studies of verbal episodic memory retrieval in neurosurgical patients (Burke et al., 2014). The mismatch in the number trials therefore made it difficult to directly compare causal signaling measures between successfully versus unsuccessfully recalled words. From the point of view of probing behaviorally effective memory encoding our focus was therefore on successful recall consistent with most prior studies (Long et al., 2014; Watrous et al., 2013). Age or gender related effects were not analyzed in our study due to lack of sufficient male participants for electrodes pairs for brain regions (for example, hippocampus-IFG and hippocampus-MFG had only two male patients each, **Table 2**).

PTE revealed significantly higher broadband causal influence of the hippocampal electrodes on the IFG and MFG electrodes than the reverse during both successful encoding and successful recall of words in the episodic memory task. Moreover, causal information flow of the hippocampus on the PFC was significantly higher during both memory encoding and recall, compared to the resting-state. Our findings are consistent with and extend a previous report in a

sample of three participants suggesting a trend towards higher causal influence of the hippocampus on bilateral PFC electrodes during episodic memory recall (Anderson et al., 2010). Using a much larger sample of 26 participants localized to the left hemisphere, we found that hippocampal influence on the PFC was significantly higher than the reverse, during both episodic memory encoding and recall. Furthermore, this pattern was observed in both the IFG and MFG subdivisions of the PFC, and causal influences of the hippocampus on the IFG and MFG did not differ from each other, neither during successful memory encoding nor during successful memory recall. Although previous fMRI studies have emphasized a greater role for the left IFG in controlled recall of verbal materials (Badre et al., 2005; Badre & Wagner, 2007; Dobbins et al., 2002; Hasegawa et al., 1999; Wagner et al., 2001), the present iEEG findings point to involvement of both the IFG and MFG. Our findings thus provide robust electrophysiological evidence for dynamic causal influence of the hippocampus on both the IFG and MFG subdivisions of the PFC during both memory encoding and recall.

Frequency-specific directionality of information flow between the hippocampus and the PFC

The second goal of our study was to investigate the frequency specificity of directional information flow between the hippocampus and the PFC. Based on previous reports in rodents and non-human primates, we focused on delta-theta (0.5-8 Hz) and beta (12-30 Hz) bands, as enhanced local field potentials in these frequency bands have been identified in the hippocampus and PFC respectively (Boran et al., 2019; Ekstrom & Watrous, 2014; Engel & Fries, 2010; Stanley et al., 2018; Watrous et al., 2013). Previous iEEG studies have reported significant delta-theta frequency (0.5-8 Hz) band activity in the hippocampus during recall of verbal, temporal

and spatial information from recently encoded memories (Foster, Kaveh, Dastjerdi, Miller, & Parvizi, 2013; Goyal et al., 2018; Jacobs et al., 2016; Solomon et al., 2019), but the frequency-specificity of causal hippocampal-PFC signaling in the human brain associated with memory encoding and recall has not been well understood. Our analysis revealed two key dissociations in the frequency specific directionality of information flow between the hippocampus and PFC.

In the delta-theta band, we found that the hippocampus had higher causal influences on the PFC, compared to the reverse direction; this pattern was observed during both verbal memory encoding and memory recall. This finding is consistent with reports of delta-theta frequency band hippocampal-PFC synchronization during spatial memory recall (Bohbot, Copara, Gotman, & Ekstrom, 2017; Ekstrom & Watrous, 2014; Watrous et al., 2013). Crucially, we extend previous reports by demonstrating directed causal influences from the hippocampus to PFC during verbal memory processing. In contrast, we found an opposite pattern in the beta band with higher PFC causal influences on the hippocampus, compared to the reverse direction; again, this pattern was observed during both memory encoding and recall.

The pattern of frequency-specific directed causal information flow observed in the present study converges surprisingly well on findings from electrocorticogram recordings in a hierarchy of left hemisphere primate visual areas (Bastos et al., 2015). In this study which involved two macaque monkeys performing a visuospatial attention task, it was found that feedforward influences were carried by delta-theta band synchronization, while feedback influences were carried by beta-band synchronization. Furthermore, theta rhythms promoted information flow in the feedforward direction during bottom-up processing while beta rhythms promoted information flow in the

reverse direction because beta influences in the top-down direction were significantly diminished when attention was directed away to the left (ipsilateral) visual field. Our findings indicate a similar pattern of frequency-specific directed causal information flow linking hierarchical inflow between the hippocampus and PFC. Top-down information flow from the PFC in the beta-band may contribute to transitioning latent neuronal ensembles into "active" representations (Spitzer & Haegens, 2017) as well as the subsequent maintenance of information in cell assemblies (Engel & Fries, 2010), while delta-theta rhythms in the hippocampus may signal pattern completion associated with memory recall that is conveyed to multiple PFC regions (Eichenbaum, 2017).

In sum, these results suggest that the hippocampus and PFC exert feedforward and feedback influences through distinct frequency channels and that delta-theta and beta rhythms have different synchronization properties. This frequency dependent directionality of information flow may provide a mechanism by which hippocampus and PFC circuits function in concert albeit via parallel signaling mechanisms pathways which reflect their distinct roles in episodic memory formation.

Phase transfer entropy, rather than power spectral density, underlies causal information flow

Phase transfer entropy, as used in the present study, provides a robust measure of direction of information flow between electrode pairs (Hillebrand et al., 2016; Lobier et al., 2014). Previous findings using multielectrode array recordings in both humans and animal models have established that phase, rather than amplitude, is crucial for both spatial and temporal encoding of

information in the brain (Kayser, Montemurro, Logothetis, & Panzeri, 2009; Lachaux, Rodriguez, Martinerie, & Varela, 1999; Lopour, Tavassoli, Fried, & Ringach, 2013; Ng, Logothetis, & Kayser, 2013; Siegel, Warden, & Miller, 2009). Consistent with this, we found no differences in overall power across the three conditions (resting-state, memory encoding, and memory recall) in any of the three brain regions – hippocampus, MFG, and IFG – examined here. Taken together, these results suggest that phase transfer entropy, rather than power spectral density, underlies causal information flow reported here.

Signal propagation and temporal delays between the hippocampus and PFC

Across all hippocampus-PFC electrode pairs, the propagation delay τ between the source and target signal estimated by the PTE analysis was 17.7 msec. τ here corresponds to the mean temporal distance between phase reversals across all electrode pairs (see **Methods**). Note that this delay refers to the embedding delay used in the PTE analysis, and does not necessarily correspond to the signal propagation delay. Nevertheless, a back of the envelope calculation indicates a close correspondence between the two. The average inter-electrode (Euclidean) distance between hippocampus and PFC electrodes in our study was 70.5 mm (actual white matter tracts will be longer). Histological studies of axonal tracts in primate lateral prefrontal cortex have suggested a conduction velocity of about 5.4 mm/msec (Caminiti et al., 2013). This results in an axonal transmission time of 13.05 msec which together with a synaptic transduction time of 3-5 msec matches the delay τ used in the PTE analysis quite well. Thus, the temporal delays used in our study are physiologically meaningful and correspond to directional hippocampus-PFC signal interactions on a timescale consistent with monosynaptic influence.

654

655 *Conclusions*

656

657 Our study advances foundational knowledge of directed information flow between the
658 hippocampus and PFC during verbal episodic memory in humans. Using high temporal
659 resolution iEEG recordings from a large cohort of participants, we uncovered distinct
660 feedforward and feedback signaling mechanisms between the hippocampus and PFC. Our study
661 also revealed frequency specificity of causal feedforward and feedback interactions between the
662 hippocampus and PFC. Our findings provide novel insights into dynamic causal interactions that
663 subserve episodic memory in the human brain and help advance knowledge of the operating
664 principles of circuit mechanisms in verbal memory encoding and recall. More broadly, our
665 findings provide a template for probing the neural circuit basis of hippocampal-PFC dysfunctions
666 which are prominent in psychiatric and neurological disorders.

667

668

669

670 **References**

671

672 Anderson, K. L., Rajagovindan, R., Ghacibeh, G. A., Meador, K. J., & Ding, M. (2010). Theta
673 oscillations mediate interaction between prefrontal cortex and medial temporal lobe in
674 human memory. *Cereb Cortex, 20*(7), 1604-1612. doi:10.1093/cercor/bhp223
675 Backus, A. R., Schoffelen, J. M., Szebenyi, S., Hanslmayr, S., & Doeller, C. F. (2016).
676 Hippocampal-Prefrontal Theta Oscillations Support Memory Integration. *Curr Biol,*
677 *26*(4), 450-457. doi:10.1016/j.cub.2015.12.048
678 Badre, D., Poldrack, R. A., Paré-Blagoev, E. J., Insler, R. Z., & Wagner, A. D. (2005).
679 Dissociable controlled retrieval and generalized selection mechanisms in ventrolateral
680 prefrontal cortex. *Neuron, 47*(6), 907-918. doi:10.1016/j.neuron.2005.07.023
681 Badre, D., & Wagner, A. D. (2007). Left ventrolateral prefrontal cortex and the cognitive control
682 of memory. *Neuropsychologia, 45*(13), 2883-2901.
683 doi:10.1016/j.neuropsychologia.2007.06.015
684 Barnett, L., & Seth, A. K. (2014). The MVGC multivariate Granger causality toolbox: A new
685 approach to Granger-causal inference. *Journal of Neuroscience Methods, 223*, 50-68.
686 doi:10.1016/j.jneumeth.2013.10.018
687 Bastos, A. M., Vezoli, J., Bosman, C. A., Schoffelen, J. M., Oostenveld, R., Dowdall, J. R., . . .
688 Fries, P. (2015). Visual areas exert feedforward and feedback influences through distinct
689 frequency channels. *Neuron, 85*(2), 390-401. doi:10.1016/j.neuron.2014.12.018
690 Benchenane, K., Peyrache, A., Khamassi, M., Tierney, P. L., Gioanni, Y., Battaglia, F. P., &
691 Wiener, S. I. (2010). Coherent theta oscillations and reorganization of spike timing in the
692 hippocampal- prefrontal network upon learning. *Neuron, 66*(6), 921-936.
693 doi:10.1016/j.neuron.2010.05.013
694 Bohbot, V. D., Copara, M. S., Gotman, J., & Ekstrom, A. D. (2017). Low-frequency theta
695 oscillations in the human hippocampus during real-world and virtual navigation. *Nat*
696 *Commun, 8*, 14415. doi:10.1038/ncomms14415
697 Boran, E., Fedele, T., Klaver, P., Hilfiker, P., Stieglitz, L., Grunwald, T., & Sarnthein, J. (2019).
698 Persistent hippocampal neural firing and hippocampal-cortical coupling predict verbal
699 working memory load. *Science Advances, 5*(3), eaav3687.
700 Brincat, S. L., & Miller, E. K. (2015). Frequency-specific hippocampal-prefrontal interactions
701 during associative learning. *Nat Neurosci, 18*(4), 576-581. doi:10.1038/nn.3954
702 Brovelli, A., Ding, M., Ledberg, A., Chen, Y., Nakamura, R., & Bressler, S. L. (2004). Beta
703 oscillations in a large-scale sensorimotor cortical network: directional influences revealed
704 by Granger causality. *Proc Natl Acad Sci U S A, 101*(26), 9849-9854.
705 doi:10.1073/pnas.0308538101
706 Burke, J. F., Sharan, A. D., Sperling, M. R., Ramayya, A. G., Evans, J. J., Healey, M. K., . . .
707 Kahana, M. J. (2014). Theta and high-frequency activity mark spontaneous recall of
708 episodic memories. *J Neurosci, 34*(34), 11355-11365. doi:10.1523/jneurosci.2654-
709 13.2014
710 Burke, J. F., Zaghloul, K. A., Jacobs, J., Williams, R. B., Sperling, M. R., Sharan, A. D., &
711 Kahana, M. J. (2013). Synchronous and asynchronous theta and gamma activity during
712 episodic memory formation. *J Neurosci, 33*(1), 292-304. doi:10.1523/JNEUROSCI.2057-
713 12.2013

714 Caminiti, R., Carducci, F., Piervincenzi, C., Battaglia-Mayer, A., Confalone, G., Visco-
715 Comandini, F., . . . Innocenti, G. M. (2013). Diameter, length, speed, and conduction
716 delay of callosal axons in macaque monkeys and humans: comparing data from histology
717 and magnetic resonance imaging diffusion tractography. *J Neurosci, 33*(36), 14501-
718 14511. doi:10.1523/jneurosci.0761-13.2013
719 Canolty, R. T., & Knight, R. T. (2010). The functional role of cross-frequency coupling. *Trends*
720 *Cogn Sci, 14*(11), 506-515. doi:10.1016/j.tics.2010.09.001
721 Croxson, P. L., Johansen-Berg, H., Behrens, T. E., Robson, M. D., Pinsk, M. A., Gross, C. G., . .
722 . Rushworth, M. F. (2005). Quantitative investigation of connections of the prefrontal
723 cortex in the human and macaque using probabilistic diffusion tractography. *J Neurosci,*
724 *25*(39), 8854-8866. doi:10.1523/JNEUROSCI.1311-05.2005
725 Cruzado, N. A., Tiganj, Z., Brincat, S. L., Miller, E. K., & Howard, M. W. (2020). Conjunctive
726 representation of what and when in monkey hippocampus and lateral prefrontal cortex
727 during an associative memory task. *Hippocampus, 30*(12), 1332-1346.
728 doi:10.1002/hipo.23282
729 Das, A., & Menon, V. (2020). Spatiotemporal Integrity and Spontaneous Nonlinear Dynamic
730 Properties of the Salience Network Revealed by Human Intracranial Electrophysiology:
731 A Multicohort Replication. *Cereb Cortex, 30*(10), 5309-5321.
732 doi:10.1093/cercor/bhaa111
733 Dickerson, B. C., & Eichenbaum, H. (2010). The episodic memory system: neurocircuitry and
734 disorders. *Neuropsychopharmacology, 35*(1), 86-104.
735 Dobbins, I. G., Foley, H., Schacter, D. L., & Wagner, A. D. (2002). Executive control during
736 episodic retrieval: multiple prefrontal processes subserve source memory. *Neuron, 35*(5),
737 989-996. doi:10.1016/s0896-6273(02)00858-9
738 Donoghue, T., Haller, M., Peterson, E. J., Varma, P., Sebastian, P., Gao, R., . . . Voytek, B.
739 (2020). Parameterizing neural power spectra into periodic and aperiodic components. *Nat*
740 *Neurosci, 23*(12), 1655-1665. doi:10.1038/s41593-020-00744-x
741 Eichenbaum, H. (2017). Prefrontal-hippocampal interactions in episodic memory. *Nat Rev*
742 *Neurosci, 18*(9), 547-558. doi:10.1038/nrn.2017.74
743 Ekstrom, A. D., & Watrous, A. J. (2014). Multifaceted roles for low-frequency oscillations in
744 bottom-up and top-down processing during navigation and memory. *Neuroimage, 85 Pt*
745 *2*, 667-677. doi:10.1016/j.neuroimage.2013.06.049
746 Engel, A. K., & Fries, P. (2010). Beta-band oscillations--signalling the status quo? *Curr Opin*
747 *Neurobiol, 20*(2), 156-165. doi:10.1016/j.conb.2010.02.015
748 Ezzyat, Y., Wanda, P. A., Levy, D. F., Kadel, A., Aka, A., Pedisich, I., . . . Kahana, M. J. (2018).
749 Closed-loop stimulation of temporal cortex rescues functional networks and improves
750 memory. *Nat Commun, 9*(1), 365. doi:10.1038/s41467-017-02753-0
751 Fan, L., Li, H., Zhuo, J., Zhang, Y., Wang, J., Chen, L., . . . Jiang, T. (2016). The Human
752 Brainnetome Atlas: A New Brain Atlas Based on Connectional Architecture. *Cereb*
753 *Cortex, 26*(8), 3508-3526. doi:10.1093/cercor/bhw157
754 Foster, B. L., Kaveh, A., Dastjerdi, M., Miller, K. J., & Parvizi, J. (2013). Human retrosplenial
755 cortex displays transient theta phase locking with medial temporal cortex prior to
756 activation during autobiographical memory retrieval. *J Neurosci, 33*(25), 10439-10446.
757 doi:10.1523/JNEUROSCI.0513-13.2013
758 Goldman-Rakic, P. S., Selemon, L. D., & Schwartz, M. L. (1984). Dual pathways connecting the
759 dorsolateral prefrontal cortex with the hippocampal formation and parahippocampal

cortex in the rhesus monkey. *Neuroscience, 12*(3), 719-743. doi:10.1016/0306-4522(84)90166-0

Goyal, A., Miller, J., Watrous, A. J., Lee, S. A., Coffey, T., Sperling, M. R., . . . Jacobs, J. (2018). Electrical Stimulation in Hippocampus and Entorhinal Cortex Impairs Spatial and Temporal Memory. *J Neurosci, 38*(19), 4471-4481. doi:10.1523/JNEUROSCI.3049-17.2018

Granger, C. W. J. (1969). Investigating Causal Relations by Econometric Models and Cross-spectral Methods. *Econometrica, 37*(3), 424-438. doi:10.2307/1912791

Greicius, M. D., Krasnow, B., Boyett-Anderson, J. M., Eliez, S., Schatzberg, A. F., Reiss, A. L., & Menon, V. (2003). Regional analysis of hippocampal activation during memory encoding and retrieval: fMRI study. *Hippocampus, 13*(1), 164-174. doi:10.1002/hipo.10064

Guitart-Masip, M., Barnes, G. R., Horner, A., Bauer, M., Dolan, R. J., & Duzel, E. (2013). Synchronization of medial temporal lobe and prefrontal rhythms in human decision making. *J Neurosci, 33*(2), 442-451. doi:10.1523/JNEUROSCI.2573-12.2013

Hasegawa, I., Hayashi, T., & Miyashita, Y. (1999). Memory retrieval under the control of the prefrontal cortex. *Ann Med, 31*(6), 380-387. doi:10.3109/07853899908998795

Hillebrand, A., Tewarie, P., van Dellen, E., Yu, M., Carbo, E. W., Douw, L., . . . Stam, C. J. (2016). Direction of information flow in large-scale resting-state networks is frequency-dependent. *Proc Natl Acad Sci U S A, 113*(14), 3867-3872. doi:10.1073/pnas.1515657113

Hoover, W. B., & Vertes, R. P. (2007). Anatomical analysis of afferent projections to the medial prefrontal cortex in the rat. *Brain Struct Funct, 212*(2), 149-179. doi:10.1007/s00429-007-0150-4

Horak, P. C., Meisenhelter, S., Song, Y., Testorf, M. E., Kahana, M. J., Viles, W. D., . . . Jobst, B. C. (2017). Interictal epileptiform discharges impair word recall in multiple brain areas. *Epilepsia, 58*(3), 373-380. doi:10.1111/epi.13633

Hutchison, R. M., Hashemi, N., Gati, J. S., Menon, R. S., & Everling, S. (2015). Electrophysiological signatures of spontaneous BOLD fluctuations in macaque prefrontal cortex. *Neuroimage, 113*, 257-267. doi:10.1016/j.neuroimage.2015.03.062

Jacobs, J., Miller, J., Lee, S. A., Coffey, T., Watrous, A. J., Sperling, M. R., . . . Rizzuto, D. S. (2016). Direct Electrical Stimulation of the Human Entorhinal Region and Hippocampus Impairs Memory. *Neuron, 92*(5), 983-990. doi:10.1016/j.neuron.2016.10.062

Jay, T. M., & Witter, M. P. (1991). Distribution of hippocampal CA1 and subicular efferents in the prefrontal cortex of the rat studied by means of anterograde transport of Phaseolus vulgaris-leucoagglutinin. *J Comp Neurol, 313*(4), 574-586. doi:10.1002/cne.903130404

Jones, M. W., & Wilson, M. A. (2005). Theta rhythms coordinate hippocampal-prefrontal interactions in a spatial memory task. *PLoS Biol, 3*(12), e402. doi:10.1371/journal.pbio.0030402

Kayser, C., Montemurro, M. A., Logothetis, N. K., & Panzeri, S. (2009). Spike-phase coding boosts and stabilizes information carried by spatial and temporal spike patterns. *Neuron, 61*(4), 597-608. doi:10.1016/j.neuron.2009.01.008

Kumaran, D., Summerfield, J. J., Hassabis, D., & Maguire, E. A. (2009). Tracking the emergence of conceptual knowledge during human decision making. *Neuron, 63*(6), 889-901. doi:10.1016/j.neuron.2009.07.030

Kuznetsova, A., Brockhoff, P. B., & Christensen, R. H. B. (2017). lmerTest Package: Tests in Linear Mixed Effects Models. *Journal of Statistical Software, 82*(13), 1-26.

Lachaux, J. P., Rodriguez, E., Martinerie, J., & Varela, F. J. (1999). Measuring phase synchrony in brain signals. *Hum Brain Mapp, 8*(4), 194-208. doi:10.1002/(sici)1097-0193(1999)8:4<194::aid-hbm4>3.0.co;2-c

Lakatos, P., Gross, J., & Thut, G. (2019). A New Unifying Account of the Roles of Neuronal Entrainment. *Curr Biol, 29*(18), R890-R905. doi:10.1016/j.cub.2019.07.075

Lam, N. H. L., Schoffelen, J. M., Udden, J., Hulten, A., & Hagoort, P. (2016). Neural activity during sentence processing as reflected in theta, alpha, beta, and gamma oscillations. *Neuroimage, 142*, 43-54. doi:10.1016/j.neuroimage.2016.03.007

Lavenex, P., & Amaral, D. G. (2000). Hippocampal-neocortical interaction: a hierarchy of associativity. *Hippocampus, 10*(4), 420-430. doi:10.1002/1098-1063(2000)10:4<420::Aid-hipo8>3.0.Co;2-5

Leopold, D. A., Murayama, Y., & Logothetis, N. K. (2003). Very slow activity fluctuations in monkey visual cortex: implications for functional brain imaging. *Cereb Cortex, 13*(4), 422-433. doi:10.1093/cercor/13.4.422

Lobier, M., Siebenhühner, F., Palva, S., & Matias, P. J. (2014). Phase transfer entropy: A novel phase-based measure for directed connectivity in networks coupled by oscillatory interactions. *NeuroImage, 85*, 853-872. doi:10.1016/j.neuroimage.2013.08.056

Long, N. M., Burke, J. F., & Kahana, M. J. (2014). Subsequent memory effect in intracranial and scalp EEG. *Neuroimage, 84*, 488-494. doi:10.1016/j.neuroimage.2013.08.052

Lopour, B. A., Tavassoli, A., Fried, I., & Ringach, D. L. (2013). Coding of information in the phase of local field potentials within human medial temporal lobe. *Neuron, 79*(3), 594-606. doi:10.1016/j.neuron.2013.06.001

Mantini, D., Perrucci, M. G., Del Gratta, C., Romani, G. L., & Corbetta, M. (2007). Electrophysiological signatures of resting state networks in the human brain. *Proc Natl Acad Sci U S A, 104*(32), 13170-13175. doi:10.1073/pnas.0700668104

Menon, V., Freeman, W. J., Cutillo, B. A., Desmond, J. E., Ward, M. F., Bressler, S. L., . . . Gevins, A. S. (1996). Spatio-temporal correlations in human gamma band electrocorticograms. *Electroencephalography and Clinical Neurophysiology, 98*(2), 89-102. doi:10.1016/0013-4694(95)00206-5

Meyer-Lindenberg, A. S., Olsen, R. K., Kohn, P. D., Brown, T., Egan, M. F., Weinberger, D. R., & Berman, K. F. (2005). Regionally specific disturbance of dorsolateral prefrontal-hippocampal functional connectivity in schizophrenia. *Arch Gen Psychiatry, 62*(4), 379-386. doi:10.1001/archpsyc.62.4.379

Miller, K. J., Weaver, K. E., & Ojemann, J. G. (2009). Direct electrophysiological measurement of human default network areas. *Proc Natl Acad Sci U S A, 106*(29), 12174-12177. doi:10.1073/pnas.0902071106

Moreno, A., Morris, R. G. M., & Canals, S. (2016). Frequency-Dependent Gating of Hippocampal-Neocortical Interactions. *Cereb Cortex, 26*(5), 2105-2114. doi:10.1093/cercor/bhv033

Moscovitch, M., Cabeza, R., Winocur, G., & Nadel, L. (2016). Episodic Memory and Beyond: The Hippocampus and Neocortex in Transformation. *Annu Rev Psychol, 67*, 105-134. doi:10.1146/annurev-psych-113011-143733

849 Neuner, I., Arrubla, J., Werner, C. J., Hitz, K., Boers, F., Kawohl, W., & Shah, N. J. (2014). The
850 default mode network and EEG regional spectral power: a simultaneous fMRI-EEG
851 study. *PLoS One, 9*(2), e88214. doi:10.1371/journal.pone.0088214
852 Ng, B. S., Logothetis, N. K., & Kayser, C. (2013). EEG phase patterns reflect the selectivity of
853 neural firing. *Cereb Cortex, 23*(2), 389-398. doi:10.1093/cercor/bhs031
854 Norman, Y., Yeagle, E. M., Harel, M., Mehta, A. D., & Malach, R. (2017). Neuronal baseline
855 shifts underlying boundary setting during free recall. *Nat Commun, 8*(1), 1301.
856 doi:10.1038/s41467-017-01184-1
857 Peterson, R. A., & Cavanaugh, J. E. (2018). Ordered quantile normalization: a semiparametric
858 transformation built for the cross-validation era. *Journal of Applied Statistics, 82*(13-15),
859 2312–2327.
860 Place, R., Farovik, A., Brockmann, M., & Eichenbaum, H. (2016). Bidirectional prefrontal-
861 hippocampal interactions support context-guided memory. *Nat Neurosci, 19*(8), 992-994.
862 doi:10.1038/nn.4327
863 Preston, A. R., & Eichenbaum, H. (2013). Interplay of hippocampus and prefrontal cortex in
864 memory. *Curr Biol, 23*(17), R764-773. doi:10.1016/j.cub.2013.05.041
865 Qin, S., Cho, S., Chen, T., Rosenberg-Lee, M., Geary, D. C., & Menon, V. (2014).
866 Hippocampal-neocortical functional reorganization underlies children's cognitive
867 development. *Nat Neurosci, 17*(9), 1263-1269. doi:10.1038/nn.3788
868 Qin, S., Duan, X., Supekar, K., Chen, H., Chen, T., & Menon, V. (2016). Large-scale intrinsic
869 functional network organization along the long axis of the human medial temporal lobe.
870 *Brain Struct Funct, 221*(6), 3237-3258. doi:10.1007/s00429-015-1098-4
871 Roy, A., Svensson, F. P., Mazeh, A., & Kocsis, B. (2017). Prefrontal-hippocampal coupling by
872 theta rhythm and by 2-5 Hz oscillation in the delta band: The role of the nucleus reuniens
873 of the thalamus. *Brain Struct Funct, 222*(6), 2819-2830. doi:10.1007/s00429-017-1374-6
874 Rugg, M. D., & Vilberg, K. L. (2013). Brain networks underlying episodic memory retrieval.
875 *Curr Opin Neurobiol, 23*(2), 255-260. doi:10.1016/j.conb.2012.11.005
876 Rutishauser, U., Reddy, L., Mormann, F., & Sarnthein, J. (2021). The Architecture of Human
877 Memory: Insights from Human Single-Neuron Recordings. *Journal of Neuroscience,*
878 *41*(5), 883-890.
879 Schoffelen, J. M., Hulten, A., Lam, N., Marquand, A. F., Udden, J., & Hagoort, P. (2017).
880 Frequency-specific directed interactions in the human brain network for language. *Proc*
881 *Natl Acad Sci U S A, 114*(30), 8083-8088. doi:10.1073/pnas.1703155114
882 Scholvinck, M. L., Maier, A., Ye, F. Q., Duyn, J. H., & Leopold, D. A. (2010). Neural basis of
883 global resting-state fMRI activity. *Proc Natl Acad Sci U S A, 107*(22), 10238-10243.
884 doi:10.1073/pnas.0913110107
885 Schreiber, T. (2000). Measuring Information Transfer. *Physical Review Letters, 85*(2), 461-464.
886 doi:10.1103/PhysRevLett.85.461
887 Schultheiss, N. W., Schlecht, M., Jayachandran, M., Brooks, D. R., McGlothan, J. L., Guilarte,
888 T. R., & Allen, T. A. (2020). Awake delta and theta-rhythmic hippocampal network
889 modes during intermittent locomotor behaviors in the rat. *Behav Neurosci*.
890 doi:10.1037/bne0000409
891 Siapas, A. G., Lubenov, E. V., & Wilson, M. A. (2005). Prefrontal phase locking to hippocampal
892 theta oscillations. *Neuron, 46*(1), 141-151. doi:10.1016/j.neuron.2005.02.028

Siegel, M., Warden, M. R., & Miller, E. K. (2009). Phase-dependent neuronal coding of objects in short-term memory. *Proc Natl Acad Sci U S A, 106*(50), 21341-21346. doi:10.1073/pnas.0908193106

Simons, J. S., & Spiers, H. J. (2003). Prefrontal and medial temporal lobe interactions in long-term memory. *Nat Rev Neurosci, 4*(8), 637-648. doi:10.1038/nrn1178

Solomon, E. A., Kragel, J. E., Sperling, M. R., Sharan, A., Worrell, G., Kucewicz, M., . . . Kahana, M. J. (2017). Widespread theta synchrony and high-frequency desynchronization underlies enhanced cognition. *Nature Communications, 8*(1), 1704. doi:10.1038/s41467-017-01763-2

Solomon, E. A., Stein, J. M., Das, S., Gorniak, R., Sperling, M. R., Worrell, G., . . . Kahana, M. J. (2019). Dynamic Theta Networks in the Human Medial Temporal Lobe Support Episodic Memory. *Curr Biol, 29*(7), 1100-1111.e1104. doi:10.1016/j.cub.2019.02.020

Spaak, E., & de Lange, F. P. (2020). Hippocampal and Prefrontal Theta-Band Mechanisms Underpin Implicit Spatial Context Learning. *J Neurosci, 40*(1), 191-202. doi:10.1523/jneurosci.1660-19.2019

Spiers, H. J. (2020). Brain rhythms that help us to detect borders. *Nature*. doi:10.1038/d41586-020-03576-8

Spitzer, B., & Haegens, S. (2017). Beyond the Status Quo: A Role for Beta Oscillations in Endogenous Content (Re)Activation. *eNeuro, 4*(4). doi:10.1523/eneuro.0170-17.2017

Stanley, D. A., Roy, J. E., Aoi, M. C., Kopell, N. J., & Miller, E. K. (2018). Low-Beta Oscillations Turn Up the Gain During Category Judgments. *Cereb Cortex, 28*(1), 116-130. doi:10.1093/cercor/bhw356

Uhlhaas, P. J., & Singer, W. (2012). Neuronal dynamics and neuropsychiatric disorders: toward a translational paradigm for dysfunctional large-scale networks. *Neuron, 75*(6), 963-980. doi:10.1016/j.neuron.2012.09.004

van Kesteren, M. T., Fernandez, G., Norris, D. G., & Hermans, E. J. (2010). Persistent schema-dependent hippocampal-neocortical connectivity during memory encoding and postencoding rest in humans. *Proc Natl Acad Sci U S A, 107*(16), 7550-7555. doi:10.1073/pnas.0914892107

Wagner, A. D., Pare-Blagoev, E. J., Clark, J., & Poldrack, R. A. (2001). Recovering meaning: left prefrontal cortex guides controlled semantic retrieval. *Neuron, 31*(2), 329-338. doi:10.1016/s0896-6273(01)00359-2

Wang, M. Y., Wang, J., Zhou, J., Guan, Y. G., Zhai, F., Liu, C. Q., . . . Luan, G. M. (2017). Identification of the epileptogenic zone of temporal lobe epilepsy from stereo-electroencephalography signals: A phase transfer entropy and graph theory approach. *Neuroimage Clin, 16*, 184-195. doi:10.1016/j.nicl.2017.07.022

Watrous, A. J., Tandon, N., Conner, C. R., Pieters, T., & Ekstrom, A. D. (2013). Frequency-specific network connectivity increases underlie accurate spatiotemporal memory retrieval. *Nature Neuroscience, 16*(3), 349-356. doi:10.1038/nn.3315

Yanagisawa, T., Yamashita, O., Hirata, M., Kishima, H., Saitoh, Y., Goto, T., . . . Kamitani, Y. (2012). Regulation of motor representation by phase-amplitude coupling in the sensorimotor cortex. *J Neurosci, 32*(44), 15467-15475. doi:10.1523/JNEUROSCI.2929-12.2012

Zhou, Y., Sheremet, A., Qin, Y., Kennedy, J. P., DiCola, N. M., Burke, S. N., & Maurer, A. P. (2019). Methodological Considerations on the Use of Different Spectral Decomposition

Algorithms to Study Hippocampal Rhythms. *eNeuro*, *6*(4). doi:10.1523/ENEURO.0142-19.2019

Figures

Figure 1. (a) iEEG recording sites in hippocampus and two prefrontal cortex subdivisions investigated in this study. (b) Event structure and timing of memory encoding and recall task phases. Participants were first presented with a list of words in the encoding block and asked to recall as many as possible from the original list after a short delay (see **Methods** for details). HIPP: hippocampus, MFG: middle frontal gyrus and IFG: inferior frontal gyrus subdivisions of prefrontal cortex.

(a) iEEG recording sites

(b) Task-structure

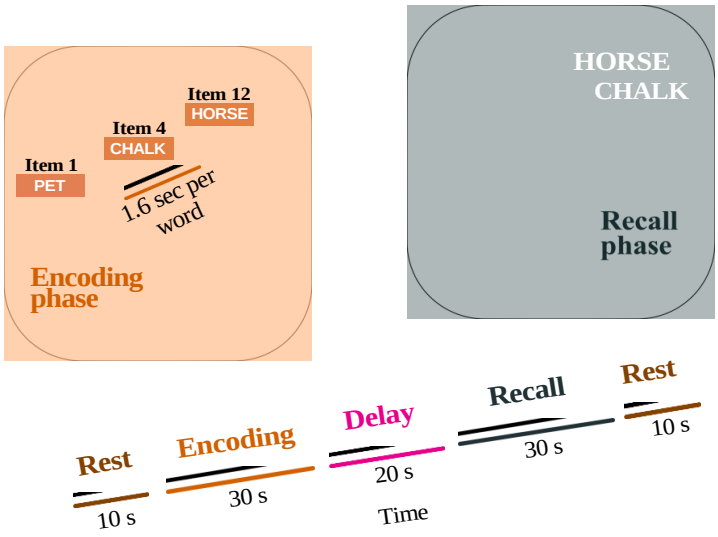

Figure 2. Causal directed information flow between hippocampus and prefrontal cortex measured using phase transfer entropy (PTE). (a) The hippocampus showed higher causal directed information flow to the IFG (HIPP → IFG) during memory encoding and recall, compared to the reverse direction (IFG → HIPP) (n=98). **(b)** The hippocampus also showed higher causal directed information flow to the MFG (HIPP → MFG) during memory encoding and recall, than the reverse direction (MFG → HIPP) (n=178). Only successfully recalled words are included. On each box, the central mark indicates the median, and the bottom and top edges of the box indicate the 25th and 75th percentiles, respectively. Whiskers extend to the most extreme data points not considered outliers. *** $p < 0.001$ (two-way ANOVA).

(a) IFG

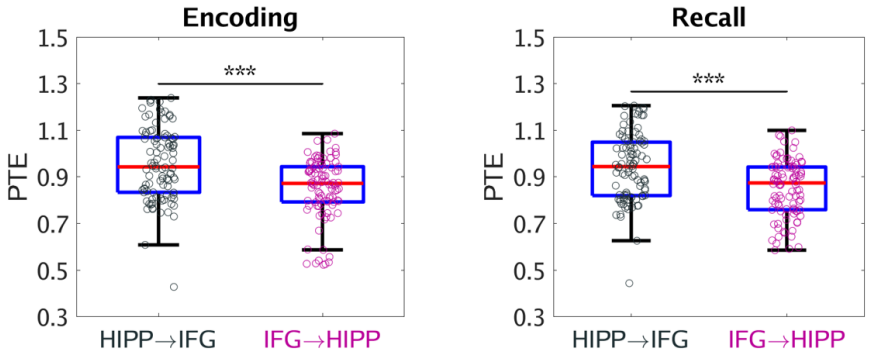

(b) MFG

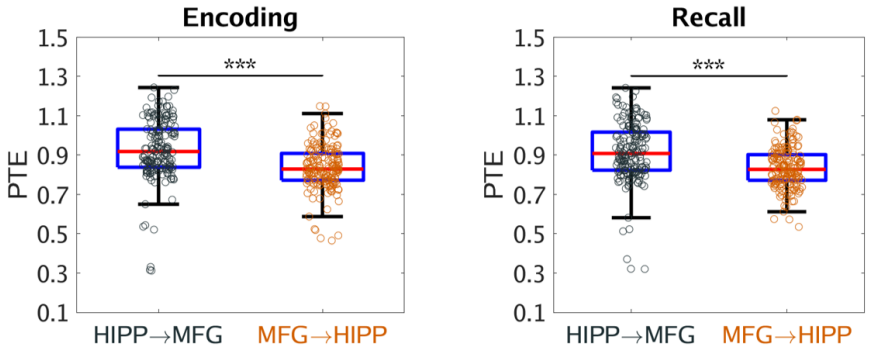

Figure 3. Causal directed information flow from HIPP to PFC during memory encoding and recall, compared to resting-state. (a) The hippocampus showed higher causal directed information flow to the IFG (HIPP → IFG) during both memory encoding and memory recall, compared to resting-state baseline (n=98). **(b)** The hippocampus also showed higher causal directed information flow to the MFG (HIPP → MFG) during both memory encoding and memory recall, compared to resting-state baseline (n=178). Only successfully recalled words are included. On each box, the central mark indicates the median, and the bottom and top edges of the box indicate the 25th and 75th percentiles, respectively. Whiskers extend to the most extreme data points not considered outliers. *** $p < 0.001$ (two-way ANOVA).

(a) IFG

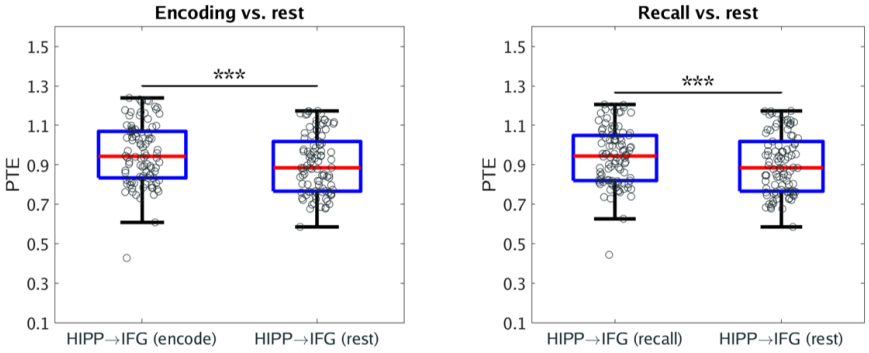

(b) MFG

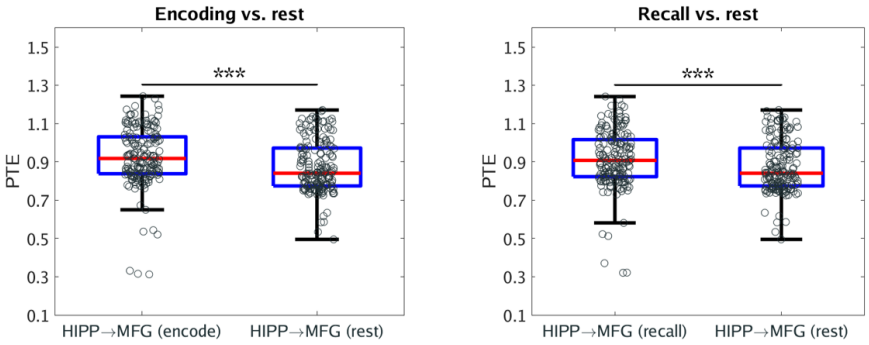

Figure 4. Causal directed information flow from hippocampus to prefrontal cortex in the delta-theta (0.5-8 Hz) frequency band. (a) Causal directed information flow from hippocampus to IFG **(**HIPP → IFG) was greater during both memory encoding and recall, compared to the reverse direction **(**IFG → HIPP) (n=98). **(b)** Similarly, causal directed information flow from hippocampus to MFG **(**HIPP → MFG) was greater during both memory encoding and recall, compared to the reverse direction **(**MFG → HIPP) (n=178). Only successfully recalled words are included. On each box, the central mark indicates the median, and the bottom and top edges of the box indicate the 25th and 75th percentiles, respectively. Whiskers extend to the most extreme data points not considered outliers. *** $p < 0.001$ (two-way ANOVA).

(a) IFG

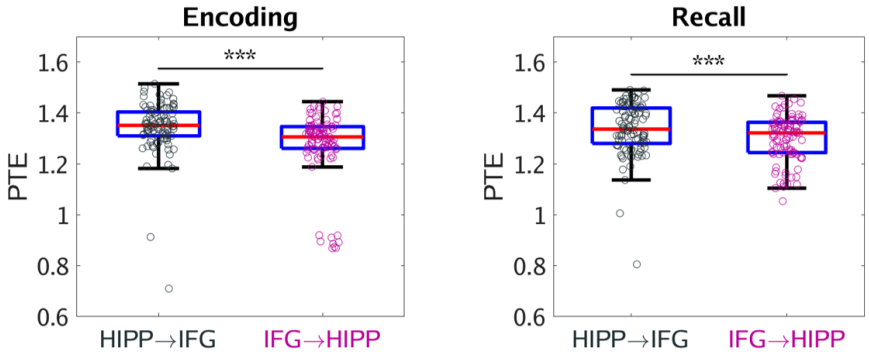

(b) MFG

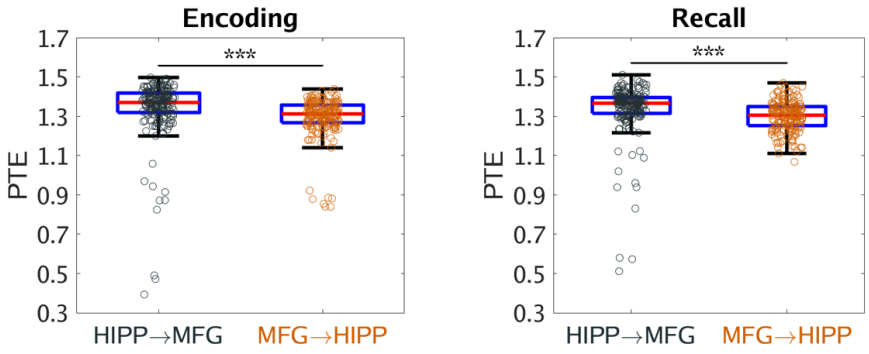

Figure 5. Causal directed information flow between hippocampus and prefrontal cortex in the delta-theta-alpha (0.5-12 Hz) frequency band. (a) Hippocampus → IFG during memory encoding and recall (n=98). **(b)** Hippocampus → MFG during memory encoding and recall (n=178). Hippocampus nodes had higher causal influences on both IFG and MFG nodes than the reverse during both memory encoding and recall in the delta-theta-alpha frequency band. Only successfully recalled words are included. On each box, the central mark indicates the median, and the bottom and top edges of the box indicate the 25th and 75th percentiles, respectively. Whiskers extend to the most extreme data points not considered outliers. *** $p < 0.001$ (two-way ANOVA).

(a) IFG

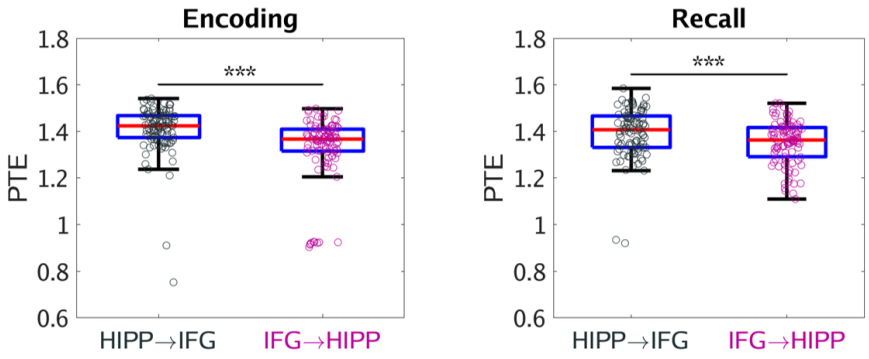

(b) MFG

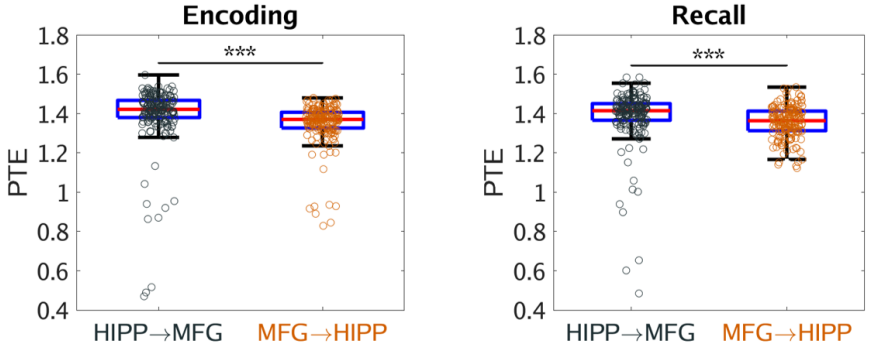

Figure 6. Causal directed information flow between hippocampus and prefrontal cortex in the beta (12–30 Hz) frequency band. (a) Hippocampus → IFG **(**HIPP → IFG) during memory encoding and recall (n=98). **(b)** Hippocampus → MFG **(**HIPP → MFG) during memory encoding and recall (n=178). Both IFG and MFG nodes had higher causal influences on the hippocampus than the reverse during both memory encoding and recall in the beta frequency band. Only successfully recalled words are included. On each box, the central mark indicates the median, and the bottom and top edges of the box indicate the 25th and 75th percentiles, respectively. Whiskers extend to the most extreme data points not considered outliers. *** $p < 0.001$, * $p < 0.05$ (two-way ANOVA).

(a) IFG

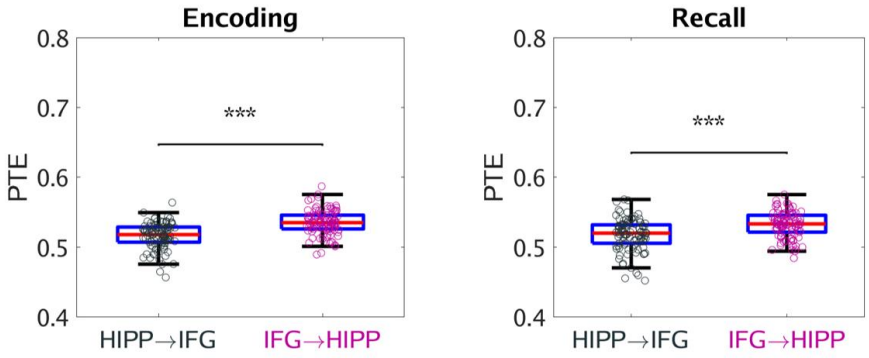

(b) MFG

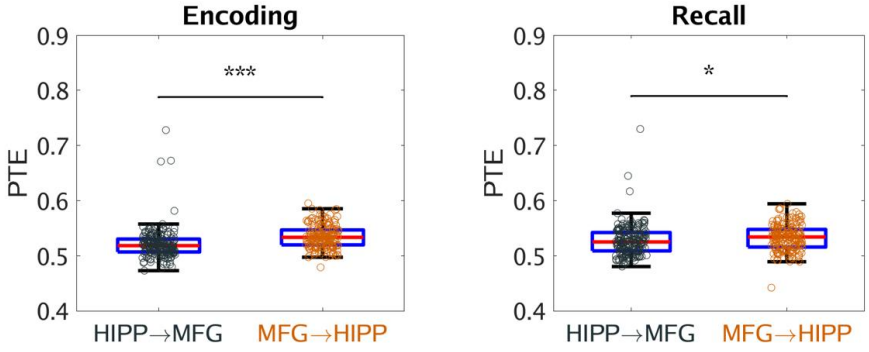

Figure 7. Surrogate data analysis to test the statistical significance of the observed PTE values compared to those obtained by chance in broadband. (a) Hippocampus → IFG **(**HIPP → IFG) during memory encoding and recall. **(b)** Hippocampus → MFG **(**HIPP → MFG) during memory encoding and recall. Shown in blue is the distribution of the surrogate PTE values and in red and green are the observed PTE for HIPP → IFG/MFG and IFG/MFG → HIPP respectively. The estimated phases from the Hilbert transform for a given pair of brain areas were time-shuffled and PTE analysis was repeated on this shuffled data to build a distribution of surrogate PTE values against which the observed PTE was tested (p<0.05).

(a) IFG

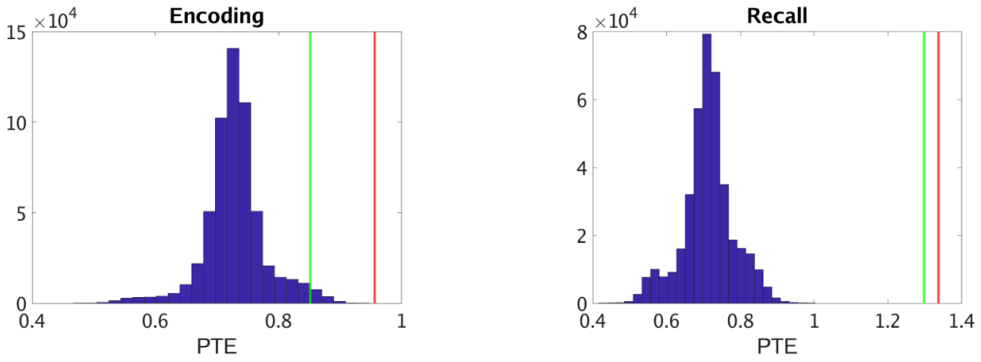

(b) MFG

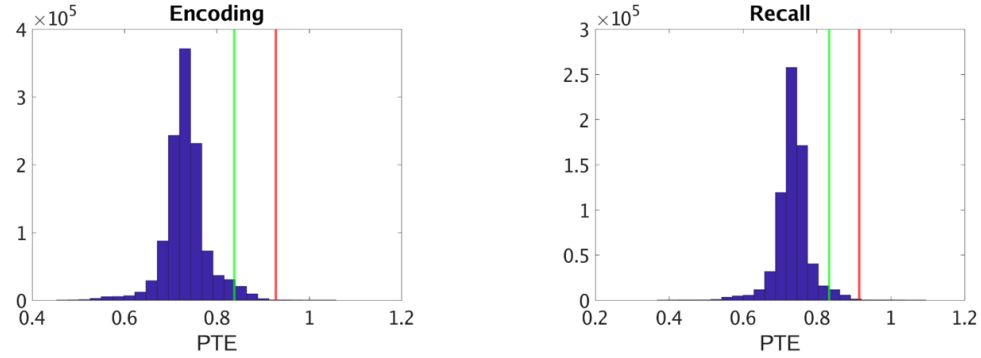

Figure 8. Surrogate data analysis to test the statistical significance of the observed PTE values compared to those obtained by chance in delta-theta band. (a) Hippocampus → IFG **(**HIPP → IFG) during memory encoding and recall. **(b)** Hippocampus → MFG **(**HIPP → MFG) during memory encoding and recall. Shown in blue is the distribution of the surrogate PTE values and in red and green are the observed PTE for HIPP → IFG/MFG and IFG/MFG → HIPP, respectively. The estimated phases from the Hilbert transform for a given pair of brain areas were time-shuffled and PTE analysis was repeated on this shuffled data to build a distribution of surrogate PTE values against which the observed PTE was tested (p<0.05).

(a) IFG

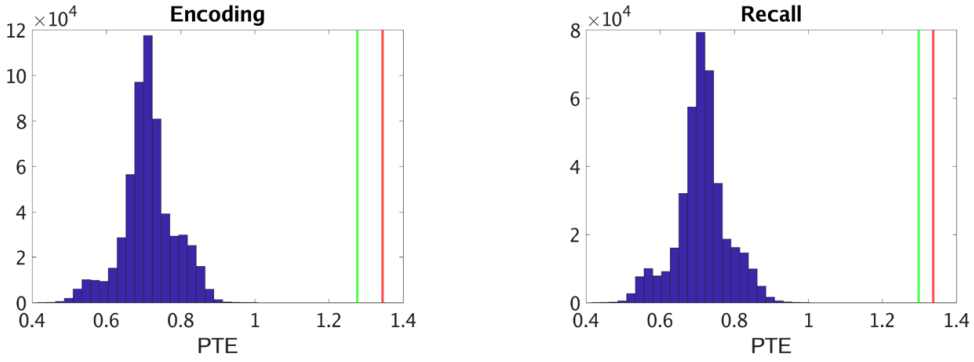

(b) MFG

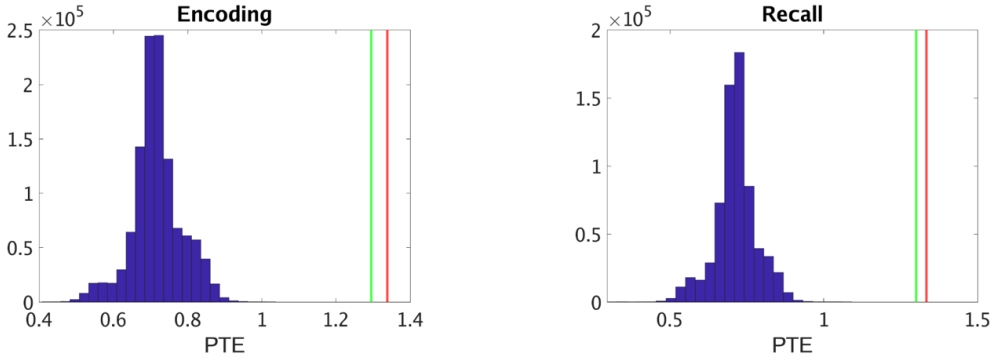

Figure 9. Surrogate data analysis to test the statistical significance of the observed PTE values compared to those obtained by chance in beta band. (a) Hippocampus → IFG **(**HIPP → IFG) during memory encoding and recall. **(b)** Hippocampus → MFG **(**HIPP → MFG) during memory encoding and recall. Shown in blue is the distribution of the surrogate PTE values and in red and green are the observed PTE for HIPP → IFG/MFG and IFG/MFG → HIPP, respectively. The estimated phases from the Hilbert transform for a given pair of brain areas were time-shuffled and PTE analysis was repeated on this shuffled data to build a distribution of surrogate PTE values against which the observed PTE was tested (p<0.05).

(a) IFG

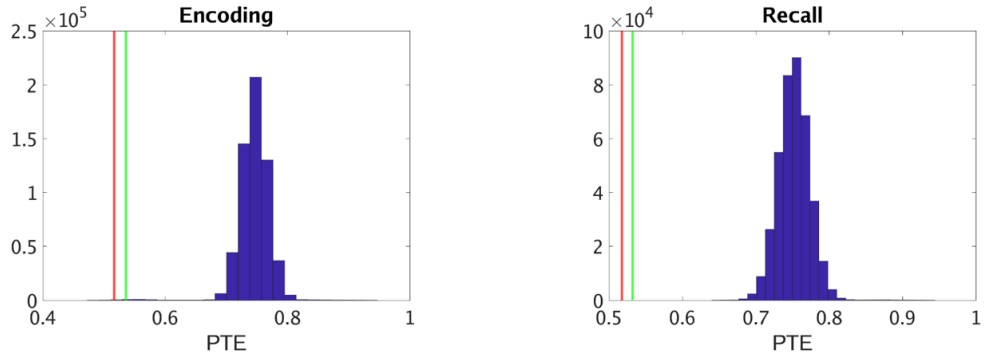

(b) MFG

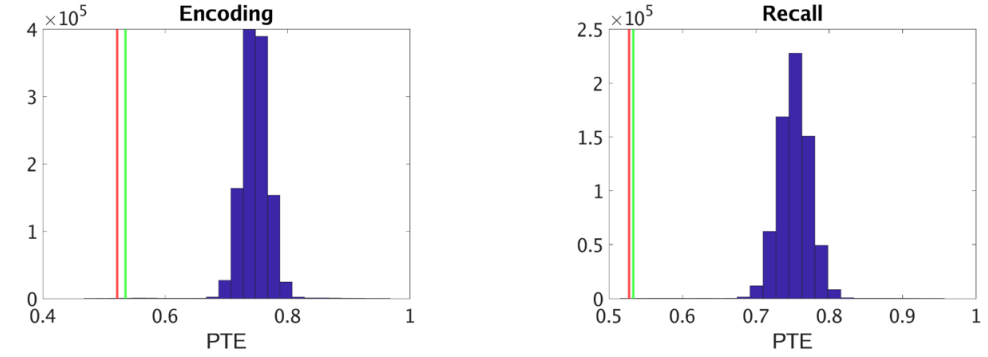

Figure 10. Spectrograms of iEEG activity during memory encoding. (a) hippocampus (n=44), **(b)** middle frontal gyrus (n=91), **(c)** inferior frontal gyrus (n=49). Red vertical line denotes presentation of word. Each word was presented for ~1.6 s. Line frequencies have been removed from y-axis and y-axis has been adjusted accordingly for visualization.

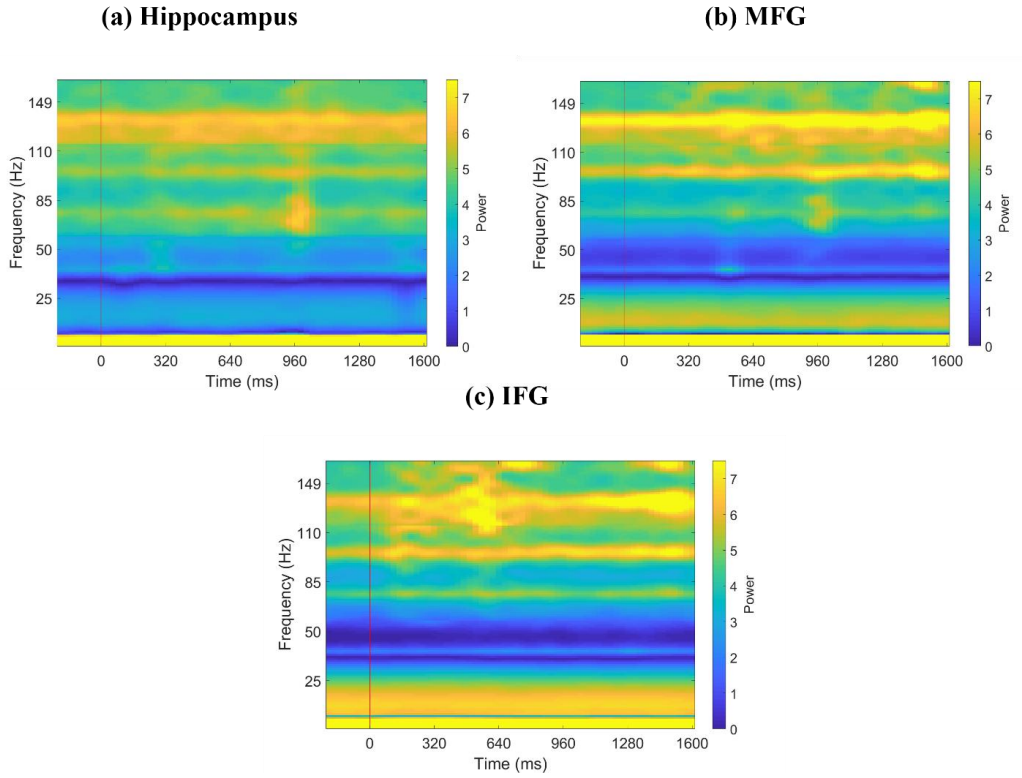

Figure 11. Spectrograms of iEEG activity during memory recall. (a) hippocampus (n=44), **(b)** middle frontal gyrus (n=94), **(c)** inferior frontal gyrus (n=49). Zero in the x-axis denotes recall of a word. Shown is 1.8 s segment immediately preceding recall of a word for each brain region. 1.6 s segment immediately preceding vocal onset of a word was considered for analysis. Line frequencies have been removed from y-axis and y-axis has been adjusted accordingly for visualization.

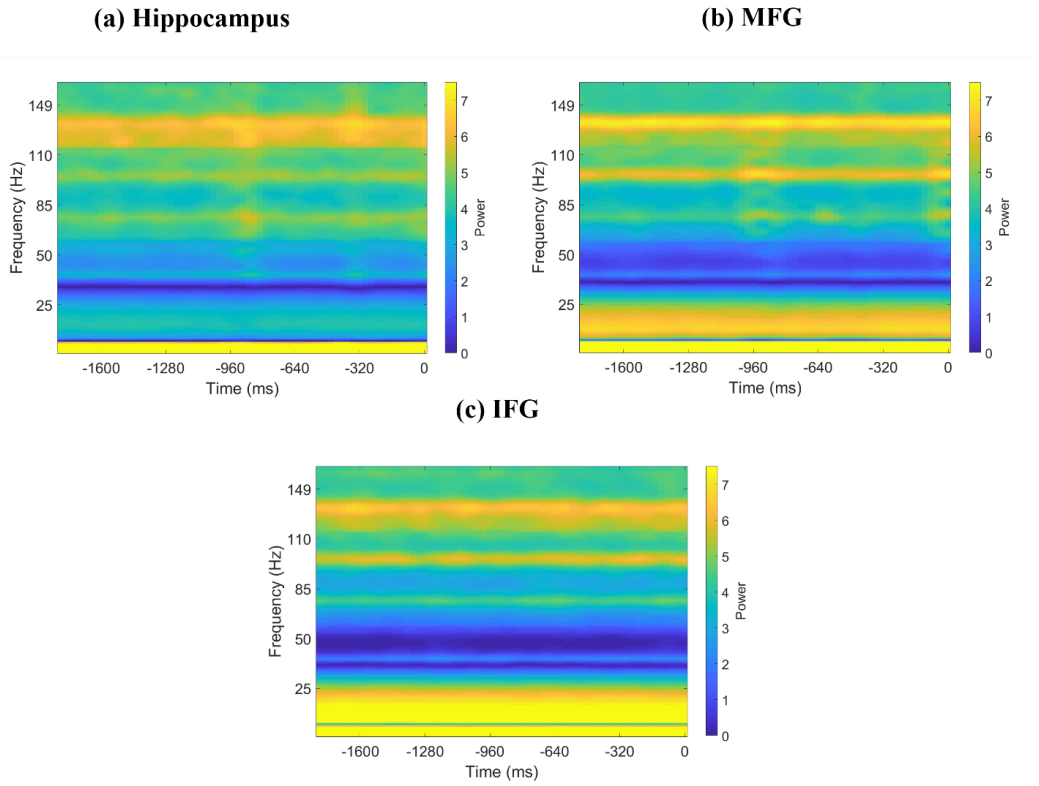

Tables

Table 1. Participant demographic information.

Participant ID	Gender	Age
185	M	20
193	M	37
195	M	44
196	M	18
200	M	25
203	F	36
204	F	25
207	F	39
222	F	20
223	F	42
228	F	58
230	F	56
232	M	27
236	F	51
240	F	37
247	F	61
260	F	57
264	F	52
275	M	41
283	F	29
286	F	57
292	F	39
297	M	24
298	F	24
299	M	43
310	M	20

Table 2. Number of electrode pairs used in phase transfer entropy (PTE) analysis. HIPP: hippocampus; IFG: inferior frontal gyrus; MFG: middle frontal gyrus.

Network pairs	Number of electrode pairs (n)	Number of participants	Participant IDs (Gender/Age)
HIPP-IFG	98	8	207 (F/39), 223 (F/42), 230 (F/56), 236 (F/51), 240 (F/37), 297 (M/24), 298 (F/24), 299 (M/43)
HIPP-MFG	178	9	195 (M/44), 207 (F/39), 223 (F/42), 228 (F/58), 230 (F/56), 240 (F/37), 247 (F/61), 298 (F/24), 299 (M/43)

Table 3. Number of electrodes in each node used in power spectral density (PSD) analysis. HIPP: hippocampus; IFG: inferior frontal gyrus; MFG: middle frontal gyrus.

Brain regions	Number of electrodes * (n)	Number of participants	Participant IDs (Gender/Age)
HIPP	44	13	195 (M/44), 203 (F/36), 207 (F/39), 223 (F/42), 228 (F/58), 230 (F/56), 236 (F/51), 240 (F/37), 247 (F/61), 292 (F/39), 297 (M/24), 298 (F/24), 299 (M/43)
IFG	49	13	200 (M/25), 204 (F/25), 207 (F/39), 223 (F/42), 230 (F/56), 236 (F/51), 240 (F/37), 260 (F/57), 264 (F/52), 286 (F/57), 297 (M/24), 298 (F/24), 299 (M/43), 310 (M/20)
MFG	94	21	185 (M/20), 193 (M/37), 195 (M/44), 196 (M/18), 200 (M/25), 204 (F/25), 207 (F/39), 222 (F/20), 223 (F/42), 228 (F/58), 230 (F/56), 232 (M/27), 240 (F/37), 247 (F/61), 260 (F/57), 264 (F/52), 275 (M/41), 283 (F/29), 286 (F/57), 298 (F/24), 299 (M/43)

*The encoding session file for subject 185 was missing. For the memory encoding task, the number of electrodes (n) was 91 for MFG.